Chemical Engineering Journal 191 (2012) 177–184

Contents lists available at SciVerse ScienceDirect

Chemical Engineering Journal

journal homepage: www.elsevier.com/locate/cej

The application of chromium substituted magnetite as heterogeneous Fenton catalyst for the degradation of aqueous cationic and anionic dyes

Xiaoliang Liang[a,b], Yuanhong Zhong[a,b], Hongping He[a,*], Peng Yuan[a], Jianxi Zhu[a], Sanyuan Zhu[a], Zheng Jiang[c]

[a] Key Laboratory of Mineralogy and Metallogeny, Guangzhou Institute of Geochemistry, Chinese Academy of Sciences, Guangzhou 510640, China
[b] Graduate School of the Chinese Academy of Sciences, Beijing 100049, China
[c] SSRF, Shanghai Institute of Applied Physics, Chinese Academy of Sciences, Shanghai 201800, China

ARTICLE INFO

Article history:
Received 1 January 2012
Received in revised form 29 February 2012
Accepted 2 March 2012

Keywords:
Chromium substituted magnetite
Heterogeneous Fenton
Degradation
Textile wastewater
Kinetics

ABSTRACT

In this study, the heterogeneous Fenton degradation of cationic and anionic dyes catalyzed by a series of Cr-containing magnetites ($Fe_{3-x}Cr_xO_4$, x = 0.00, 0.18, 0.33, 0.47 and 0.67) has been investigated under neutral pH conditions. Methylene blue (MB) and acid orange II (AOII) were chosen as models of cationic and anionic contaminants. Emphases were laid on the comparison of degradation characteristic between MB and AOII and the effect of Cr substitution on the degradation efficiency of both dyes. The octahedral occupancy of Cr^{3+} increased the BET surface area and superficial hydroxyl amount of magnetite, resulting in an improvement of adsorption ability of MB. However, these Cr-containing magnetites showed no adsorption to AOII. The MB degradation, following the Langmuir–Hinshelwood model, was well fitted by zero-order equation while AOII degradation following the Eley–Rideal model, was well fitted with two-stage pseudo-first-order kinetics. The Cr incorporation significantly improved the catalytic activity of magnetite in heterogeneous Fenton reaction, but the extent of improvement varied with the substitution level. These new insights are of high importance for the environmental application of metal substituted magnetites in the purification of textile wastewater.

1. Introduction

The growing interest in the application of transition metal substituted magnetites as heterogeneous Fenton catalysts in the degradation of organic pollutants (e.g. dyes, phenol and hydroquinone) has been evoked in the past few years [1–4], due to high degradation efficiency around neutral pH, easy recycle of catalyst in practical wastewater purification [5] and prevalence as natural minerals on the earth surface [6]. So far, several metal cations, such as Ti^{4+} [7], V^{3+} [8], Mn^{2+} [4], Co^{2+} [4] and Cr^{3+} [3], have been reported as active components to increase the Fenton catalytic activity of magnetite. It has been widely acknowledged that the catalytic activity of magnetite is greatly dependent on the species, valence and occupancy of substituting metals [9–11]. Substituting metals exhibiting thermo-dynamically favorable redox pairs (e.g. Co^{2+}/Co^{3+}) can improve the catalytic activity of magnetite by accelerating the electronic transfer to produce the active species Fe^{2+} for the Fenton reaction [1]. The catalytic activity relies on the octahedral cations rather than the tetrahedral ones, as the octahedral sites are almost exclusively exposed at the surface of the spinel structure (Fig. 1) [12]. These experimental evidences have greatly promoted the application of transition metal substituted magnetites in environmental engineering.

In the studies on Fenton catalytic activity of substituted magnetites, cationic dye, methylene blue (MB) is the mostly used model pollutant. Oliveira and co-workers investigated the individual effect of Mn, Co and Cr substitution on the Fenton catalytic activity of magnetite for MB degradation [1,3]. It was concluded that these substitution remarkably improved the MB degradation, ascribed to the increase of catalytic activity for H_2O_2 decomposition. However, the changes of adsorption and its influence on degradation efficiency were unexpectedly neglected. In fact, these substituted cations increased the amount of surface hydroxyl. Under the studied neutral pH, since the point of zero charge (PZC) of magnetite is about 6.8, the increase of surface hydroxyl amount would certainly enhance the cationic MB adsorption on magnetite surface with negative charge through electrostatic interaction (Eqs. (1) and (2)) [13,14]. As comfirmed by previous research [15,16], the increase of dye adsorption accelerates its degradation. Therefore,

* Corresponding author. Present address: Key Laboratory of Mineralogy and Metallogeny, Guangzhou Institute of Geochemistry, Chinese Academy of Sciences, 511 Kehua Street, Guangzhou, 510640, China. Tel.: +86 20 85290257; fax: +86 20 85290708.
E-mail address: hehp@gig.ac.cn (H. He).

1385-8947/$ – see front matter © 2012 Elsevier B.V. All rights reserved.
doi:10.1016/j.cej.2012.03.001

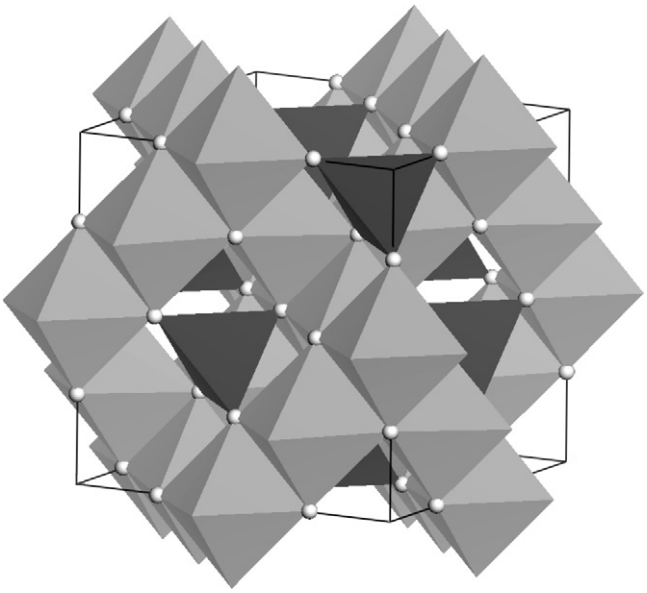

Fig. 1. The unit cell of magnetite.

the variation of adsorption should not be ignored while investigating the effect of metal substitution on catalytic activity of magnetites.

$$M{-}OH + {}^{-}OH \leftrightarrow M{-}O^{-} + H_2O \quad (1)$$

$$M{-}O^{-} + {}^{+}MB \leftrightarrow M{-}O^{-}{}^{+}MB \quad (2)$$

The adsorption behavior is closely related to not only the surface properties of adsorbent, but also the pollutant characters. Based on the significant effect of adsorption on degradation process, the influence of pollutant type should inevitably be regarded while testing the catalytic activity. To the best of our knowledge, transition metal substituted magnetites have been available as Fenton catalysts in the degradation of cationic dye (e.g. MB), but they have seldom been tested in anionic dye decomposition. Moreover, comparison of degradation characteristics between cationic and anionic dyes in this kind of heterogeneous Fenton reaction system has hardly been systematically researched. These two problems are certainly not good for the application of substituted magnetites in the purification of textile wastewater.

In the current study, the applicability of substituted magnetite as Fenton catalyst in the degradation of cationic (MB) and anionic (acid orange II) model dyes was investigated. pH was selected at neutral condition to avoid the iron leaching and occurrence of homogeneous Fenton reaction. Due to the prevalence of chromium substitution in the natural magnetite minerals [17], chromium substituted magnetite ($Fe_{3-x}Cr_xO_4$) was chosen as the example of substituted magnetites. As prolonged exposure to Cr(III) species could cause skin allergies and cancer in human beings [18], chromium dissolution was tracked during the dye degradation. MB ($pK_a > 12$) is a heterocyclic aromatic chemical compound with the molecular formula $C_{16}H_{18}N_3SCl$ (Fig. 2A) [19]. Acid orange II (AOII, $pK_{a1} = 1.0$, $pK_{a2} = 11.4$) is an anionic dye with the formula $C_{16}H_{11}N_2NaO_4S$ (Fig. 2B), which is usually chosen as one of the model azo dyes in literature [20,21]. Azo dyes are a major class of synthetic colored organic compounds that account for about half of the textile dyestuffs used today [22]. The main object of the present study is to make the comparison of degradation characteristics between cationic and anionic model dyes in heterogeneous Fenton reaction and elucidate the effect of metal substitution on the degradation efficiency of both two dyes by magnetites. The new insights obtained in this study are of high importance for application of natural magnetites in pollution controlling and environmental remediation.

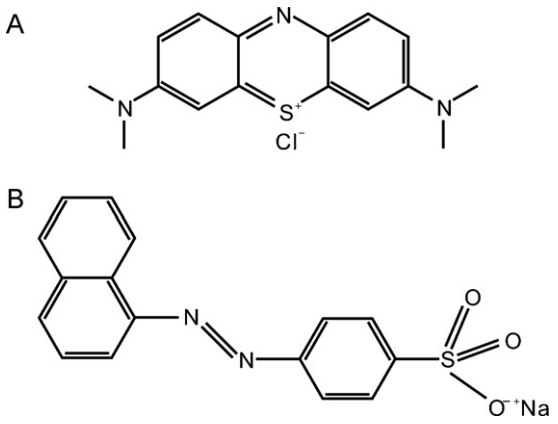

Fig. 2. The structural formula for: (A) methylene blue and (B) acid orange II.

2. Experimental

2.1. Preparation of $Fe_{3-x}Cr_xO_4$

All chemicals and reagents used in this work were of analytical grade and used as received. Magnetite samples with different Cr substitution extent were prepared by using a precipitation–oxidation method [23]. Predetermined amounts of $FeSO_4{\cdot}7H_2O$ and $CrCl_3{\cdot}6H_2O$ were dissolved in HCl solution (total metal cation concentration was about 0.90 mol L^{-1}). 1.0 mL hydrazine was added to prevent the oxidation of Fe^{2+} cations, and pH was low enough (<1) to prevent Fe^{2+} oxidation and hydroxide precipitation. This solution was heated to 90–100 °C. Equal volume of a solution containing 4.0 mol L^{-1} NaOH and 0.90 mol L^{-1} $NaNO_3$ was added dropwise (10 mL min^{-1}) into the heated iron solution and the reaction was maintained at 90 °C for 2 h, while stirring at a rate of 500 rpm. Then, the solution was cooled to room temperature. It was necessary to emphasize that during the reaction, N_2 was passed through to prevent the oxidation of Fe^{2+} by air. The particles were then separated by centrifugation at 3500 rpm for 5 min and washed with boiling distilled water, followed by an additional centrifugation. After 3–4 washings, the particles were collected and dried in a vacuum oven at 100 °C for 24 h. Also, Fe_3O_4 was synthesized using the above procedure without adding $CrCl_3{\cdot}6H_2O$. All the samples were ground and passed through a 200 mesh screen.

2.2. Characterization of $Fe_{3-x}Cr_xO_4$

The chemical composition of $Fe_{3-x}Cr_xO_4$ was obtained by chemical analyses. The contents of Fe and Cr in the prepared samples were determined spectrophotometrically by the phenanthroline and 1, 5 diphenylcarbohydrazide methods. The value of x in the formula $Fe_{3-x}Cr_xO_4$ was obtained from the chemical analysis results.

Power X-ray diffraction (PXRD) were recorded between 10° and 80° (2θ) at a step of 1° min^{-1} using a Bruker D8 advance diffractometer with Cu Kα radiation (40 kV and 40 mA).

Specific surface area measurements were carried out by using the BET method on the basis of the N_2 physisorption capacity at 77 K on an ASAP 2020 instrument. All the samples were degassed at 433 K for 12 h before test.

The PZC of magnetite samples was detected by the potentiometric titration (PT) method [24]. The sample was mixed with NaCl solutions of different concentrations (c) to obtain 1 g L^{-1} magnetite suspensions in which the final concentrations of NaCl are 0.001, 0.010, and 0.100 mol L^{-1}. When the change in pH value did not

exceed 0.02 pH unit in 5 min, the amount of acid or base added and the potential value of the suspension were recorded and used to calculate the adsorption amounts of H^+ and OH^-. Finally, PT curves were obtained by plotting (OH^- and H^+) versus pH for different c values.

The Cr K-edge X-ray absorption near-edge structure (XANES) spectra of $Fe_{3-x}Cr_xO_4$ samples and reference compounds were collected at Shanghai Synchrotron Radiation Facility (SSRF), on the new Wiggler beamline BL14W1. The storage ring operating conditions were 3.5 GeV electron energy and 150–300 mA electron current. The used beam size at the sample position was about 200 μm × 200 μm. A Si (1 1 1) double crystal monochromator was used in these experiments. XANES data for all the samples was collected in the transmission mode. Data analyses were performed using IFEFFIT software package. All the spectra have been normalized to eliminate the influence of the target element content. The absorption edge is defined as the maximum of derivative at the absorption edge.

Thermogravimetric (TG) analyses were performed on a Netzsch STA 409 PC Instrument. About 20 mg of finely ground sample was heated in a corundum crucible from 30 to 1000 °C at a heating rate of 10 °C min^{-1} under N_2 atomosphere (60 cm^3 min^{-1} at normal temperature and pressure).

2.3. Catalytic activity test of $Fe_{3-x}Cr_xO_4$

The heterogeneous Fenton degradation experiments were carried out in a conical flask (containing 250 mL of reaction solution) at 25 °C. The dosage of catalyst was 1.0 g L^{-1} while the concentrations of model dye (MB or acid orange II) and H_2O_2 were 0.2 and 80 mmol L^{-1}. All the experiments were carried out under constant stirring to make the catalyst well dispersed. The initial pH 7.0 of solution was adjusted by H_2SO_4 and NaOH. Before adding H_2O_2, the suspension containing catalyst and dye was stirred for 1 h, predetermined time for achieving adsorption equilibrium (Fig. S-1). Then the degradation reaction was initiated by adding H_2O_2 into the dye solution. At given intervals of degradation, an aliquot of 3.0 mL solution was taken out and immediately treated with equal volume of prepared stabilizing reagent. The prepared stabilizing reagent contained 0.1 mol L^{-1} Na_2SO_3 and 0.05 mol L^{-1} NaOH [25,26]. The sample was then centrifuged for 3 min and the supernatant was analyzed by UV–vis spectroscopy UV-7504 at λ_{max} = 665 nm for MB, and λ_{max} = 484 nm for AOII. Different H_2O_2 concentrations (80, 64, 48, 32 and 16 mmol L^{-1}) and different initial pH (3.0, 5.0, 7.0 and 9.0) were tested for AOII degradation, without changing other parameters as mentioned above.

The pH of reaction system was monitored by a PHS-3C pH meter (Rex Instrument Factory, Shanghai, China). The concentrations of leaching Fe and Cr ions during the degradation were determined on a PE-3100 flame atomic absorption spectrophotometer (FAAS) with the hollow-cathode lamps operate at the wavelength of 248.3 and 357.9 nm.

3. Results and discussion

3.1. Characterization of $Fe_{3-x}Cr_xO_4$

From the chemical analysis results (Table 1), it can be seen that the proportion between chromium and iron contents increases with the increase of chromium substitution extent, indicating the substitution of Cr for Fe. The chemical formulae of all the prepared samples calculated from the chemical analysis results are also shown in Table 1.

The XRD patterns of $Fe_{3-x}Cr_xO_4$ (Fig. 3) well correspond to the standard card of magnetite (JCPDS: 19-0629), confirming that all

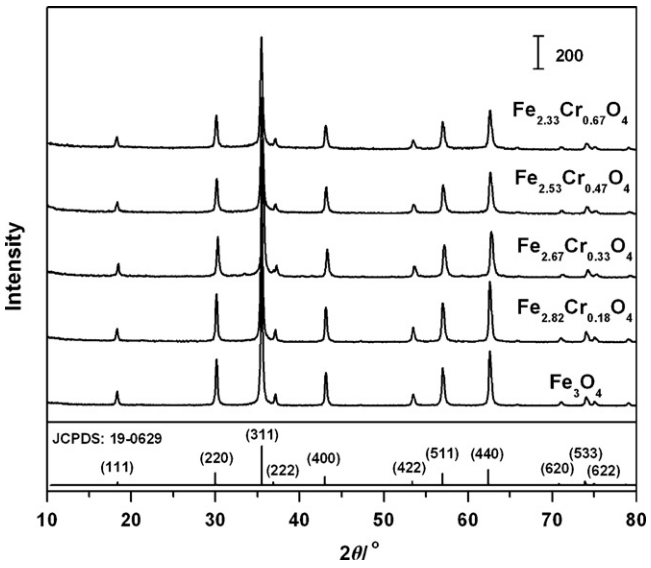

Fig. 3. XRD patterns for the series $Fe_{3-x}Cr_xO_4$.

the prepared samples have spinel structure. Table 1 also shows the lattice parameter a_0, crystal size, BET specific surface area and PZC of $Fe_{3-x}Cr_xO_4$. The Cr substitution does not obviously change the lattice parameter a_0 and crystal size. But the specific surface area obviously increases with the increment of Cr content.

XANES characterization was carried out to probe the valence and occupancy of chromium in $Fe_{3-x}Cr_xO_4$ structure (Fig. 4). Compared to the traditional techniques of FTIR and Mössbauer spectroscopy that just provide the structural changes of iron and do not reflect the occupancy changes of the substituting cations with enough precision, XANES can in situ probe the coordinated environment of the target cations [27,28]. The pre-edge and absorption edge position values of the spectra in Fig. 4 are summarized in Table 2. For Cr^0 in Co foil, Cr^{3+} in Cr_2O_3 and Cr^{6+} in CrO_3, their energy positions of absorption edges shift to higher energy value with the increasing valence (Table 2). For octahedral Cr^{3+} in normal spinel $FeCr_2O_4$, its

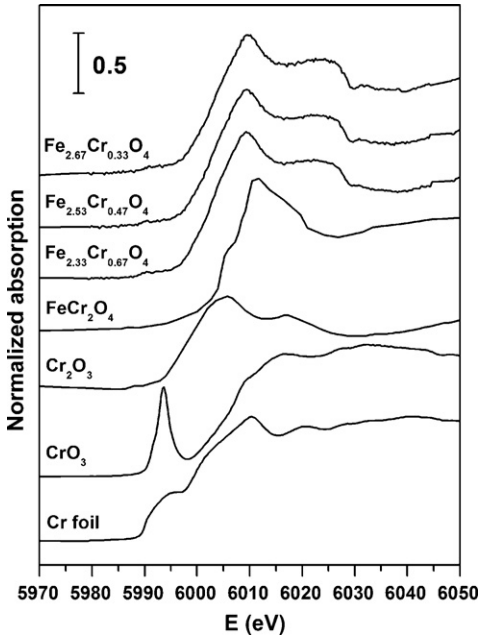

Fig. 4. Cr K-edge XANES spectra of Cr foil, Cr_2O_3, CrO_3, $FeCr_2O_4$ and series $Fe_{3-x}Cr_xO_4$.

Table 1
Chemical analyses, lattice parameter a_0, crystal size, specific surface area and PZC of $Fe_{3-x}Cr_xO_4$.

Samples	Chemical analyses Cr/Fe	Lattice parameter a_0 (nm)	Crystal size (nm)	Specific surface area ($m^2\ g^{-1}$)	PZC
Fe_3O_4	0	8.411	43	27.84	6.82
$Fe_{2.82}Cr_{0.18}O_4$	0.060	8.391	25	61.94	6.74
$Fe_{2.67}Cr_{0.33}O_4$	0.114	8.406	27	88.60	6.75
$Fe_{2.53}Cr_{0.47}O_4$	0.173	8.394	32	76.71	6.69
$Fe_{2.33}Cr_{0.67}O_4$	0.266	8.384	26	111.92	6.79

Table 2
The pre-edge and absorption edge position value for Cr K-edge XANES spectra of $Fe_{3-x}Cr_xO_4$ and reference samples.

Materials	E (Pre-edge) (eV)	E (Edge) (eV)
Cr foil	No peak	5989.2
Cr_2O_3	5987.7	5998.5
CrO_3	5993.7	6007.2
$FeCr_2O_4$	5987.8	6000.5
$Fe_{2.67}Cr_{0.33}O_4$	5990.2	6000.7
$Fe_{2.53}Cr_{0.47}O_4$	5990.2	6000.7
$Fe_{2.33}Cr_{0.67}O_4$	5990.2	6000.7

absorption edge position is close to that of Cr^{3+} in Cr_2O_3. For Cr cations in $Fe_{3-x}Cr_xO_4$, their K-edge positions are also quite close to those of Cr^{3+} in Cr_2O_3 and $FeCr_2O_4$, but far from those of CrO_3 and Cr metal (Table 2). Moreover, the peak profiles of $Fe_{3-x}Cr_xO_4$ are also similar to that of spinel $FeCr_2O_4$ containing octahedral Cr^{3+}. These two evidences indicate that Cr cations in $Fe_{3-x}Cr_xO_4$ are mainly Cr^{3+}.

The intensity of the pre-edge peak varies with the coordination environment of the target element [29,30]. For Cr foil, Cr atoms have a cubic symmetry and its XANES spectrum does not show any pre-edge peak (Fig. 4 and Table 2). For α-Cr_2O_3 with Cr atom occupying a distorted octahedral site [31], its XANES spectrum shows a weak pre-edge peak (Fig. 4). By contrast, for CrO_3 where Cr atom occupies a distorted tetrahedral site, a strong pre-edge peak can be observed. In the case of chromite ($FeCr_2O_4$) with normal spinel structure, Cr^{3+} cation occupies a distorted octahedral site and its pre-edge peak is quite weak [32]. The quite weak pre-edge peaks of Cr^{3+} in $Fe_{3-x}Cr_xO_4$ suggest that Cr^{3+} mainly occupy the octahedral sites rather than tetrahedral ones.

Under N_2 atmosphere, two mass losses are recorded in the TG curves for all the $Fe_{3-x}Cr_xO_4$ samples (Fig. 5). The first mass loss, observed from ca. 30 to 120 °C, corresponds to the dehydration, while the other one, from ca. 150 to 500 °C, is assigned to the dehydroxylation [33]. Obviously, the mass loss resulted from the dehydroxylation increases with the increase of the chromium substituting level, indicating that the Cr incorporation increases the surface hydroxyl amount of magnetite. The surface hydroxyl (—OH) groups are functional groups of iron oxides and have a vital influence on surface adsorption [34], photocatalysis [35] and surface acidity (Brønsted acid) [36]. The overall density of surface hydroxyl is related to the crystal structure and extent of the development of different crystal faces [37]. From XANES results, the incorporation of chromium results in a slight distortion of the magnetite lattice, leads to the increase in surface hydroxyl amount [38].

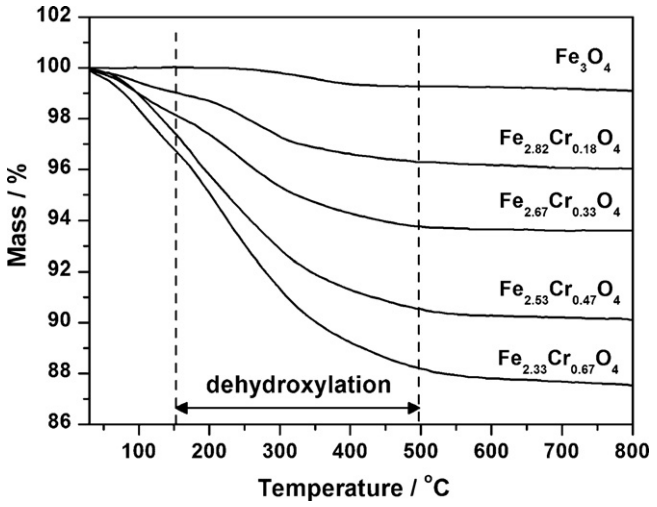

Fig. 5. Thermogravimetric profiles of $Fe_{3-x}Cr_xO_4$ samples under N_2.

3.2. Catalytic activity test of $Fe_{3-x}Cr_xO_4$

3.2.1. Decolorization of MB and AOII

Fig. 6 shows the degradation processes of cationic (MB) and anionic (AOII) model dyes through heterogeneous Fenton reaction catalyzed by series of $Fe_{3-x}Cr_xO_4$ around neutral pH. Before adding H_2O_2, the decolorization of model dyes only relied on the adsorption by $Fe_{3-x}Cr_xO_4$. For MB, its removal rate was 2.4%, 3.2%, 15.3%, 22.0% and 25.0% through the adsorption by Fe_3O_4, $Fe_{2.82}Cr_{0.18}O_4$, $Fe_{2.67}Cr_{0.33}O_4$, $Fe_{2.53}Cr_{0.47}O_4$ and $Fe_{2.33}Cr_{0.67}O_4$, respectively, increasing with the increment of Cr substitution level (Fig. 6A). But for AOII, its removal rate by adsorption was quite low (<1%) and did not show obvious variation when the catalysts contained different Cr contents (Fig. 6B). This completely different adsorption behaviors of MB and AOII on $Fe_{3-x}Cr_xO_4$ was attributed to the surface charge of magnetite. According to the pH_{pzc} of $Fe_{3-x}Cr_xO_4$ (Table 1) and the $pK_a > 12$ of MB, the investigated magnetites were with weakly negative charge and MB existed as cations at neutral pH, resulting in a strong positive-charge-induced dipole–dipole interaction with a weak electrostatic interaction between magnetite and MB. The negative surface charge increased with the increment of superficial hydroxyl and the later was positively related with the amount of incorporated metals as indicated by thermal analysis. Accordingly, the quantity of adsorbed MB cations obviously increased with the amount of chromium incorporated in magnetites [39,40]. However, for AOII, whose pK_{a1} is 1.0 for the $-SO_3H$ group and pK_{a2} is 11.4 for the naphthalene of AOII, most of the dye existed as anions in the studied pH. The weak negatively charged surface was not favorable for its adsorption on magnetite, while the charge induced dipole–dipole interaction was a weak interaction caused by negatively charged groups of anions.

After adding H_2O_2 into the system, the dye decolorization depended on Fenton degradation and the removal rate increased with the reaction time. After 200 min of degradation, the MB removal rate was 59.3%, 71.3%, 87.0% and 95.2% in the presence of $Fe_{2.82}Cr_{0.18}O_4$, $Fe_{2.67}Cr_{0.33}O_4$, $Fe_{2.53}Cr_{0.47}O_4$ and $Fe_{2.33}Cr_{0.67}O_4$, respectively. No obvious decolorization was observed in the system only containing H_2O_2 but no magnetite (Fig. 6A). Therefore, the incorporation of Cr enhanced the MB decolorization.

The effect of Cr substitution on AOII decolorization looked similar to that on MB decolorization. H_2O_2 solely or with Fe_3O_4 did not engender obvious AOII decolorization (Fig. 6B). But with $Fe_{2.82}Cr_{0.18}O_4$, $Fe_{2.67}Cr_{0.33}O_4$, $Fe_{2.53}Cr_{0.47}O_4$ and $Fe_{2.33}Cr_{0.67}O_4$, about 48.6%, 81.6%, 86.4% and 89.6% of AOII was removed after 240 min, respectively. It can be seen that Cr substitution in

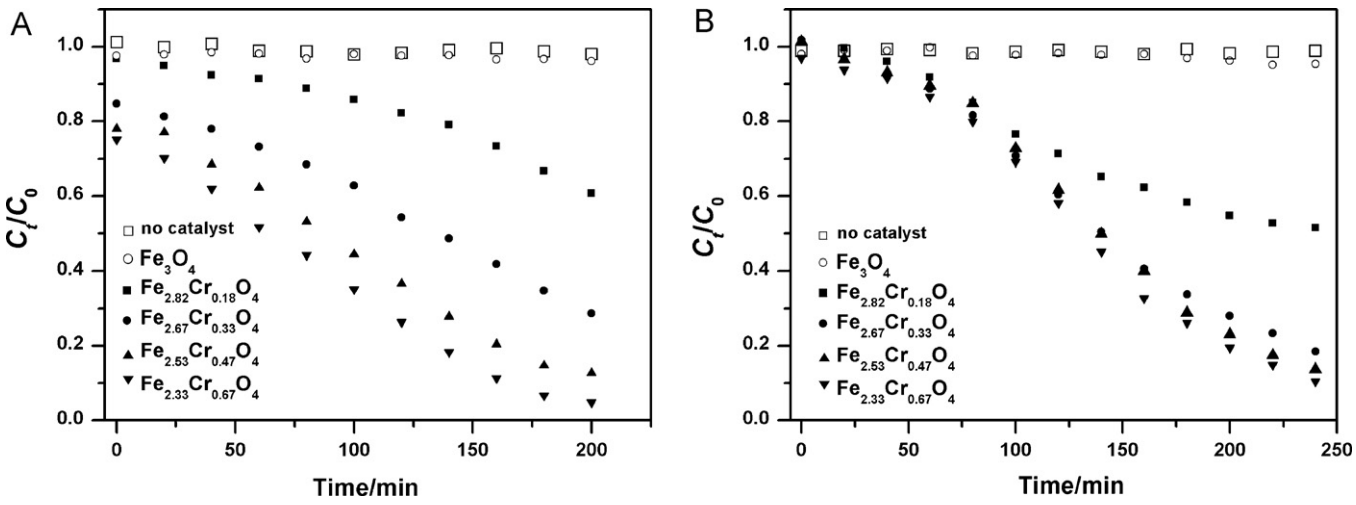

Fig. 6. Decolorization of (A) methylene blue and (B) acid orange II through heterogeneous Fenton reaction catalyzed by $Fe_{3-x}Cr_xO_4$ (C_0 = 0.2 mmol L^{-1}, 80 mmol L^{-1} of H_2O_2, 1.0 g L^{-1} of catalyst, 250 mL, pH 7.0, 25 °C).

magnetite greatly increased the decolorization of both MB and AOII through Fenton reaction. During the degradation, the pH was above 5.5 and the concentrations of dissolved Fe and Cr were below 0.5 mg L^{-1}, indicating that the dissolution of Fe and Cr ions can be ignored and the whole decomposition of MB and AOII was heterogeneous Fenton reaction [41,42].

3.2.2. Degradation kinetics

The degradation processes in Fig. 6 were analyzed in terms of kinetics. Previous studies have indicated that the degradation of dye in Fenton reaction follows the hydroxyl radical-mediated mechanism, in which hydroxyl radicals (•OH) are generated by the reaction between H_2O_2 and catalyst and then attack the dye molecules [43,44]. The rate of •OH production can reflect the catalytic activity of Fenton catalyst. Based on the observed adsorption of MB on $Fe_{3-x}Cr_xO_4$, the Fenton degradation of MB in this study followed the Langmuir–Hinshelwood mechanism (i.e. reaction of adsorbed MB molecule with •OH engendered on magnetite surface, Eq. (3)) [45,46], which is typically described as a second-order reaction (Eq. (4)):

$$\equiv\text{M—OMB} + [^{\bullet}\text{OH}]_{\text{surf}} \rightarrow \text{products} \quad (3)$$

$$\frac{d[\equiv\text{M–OMB}]}{dt} = -k[\equiv\text{M–OMB}][^{\bullet}\text{OH}]_{\text{surf}} \quad (4)$$

where [≡M—OMB] is the adsorbed amount of MB on $Fe_{3-x}Cr_xO_4$, $[^{\bullet}OH]_{surf}$ is the concentration of •OH on magnetite surface, k is the second order rate constant, and t is the degradation time. In the present study, the addition of H_2O_2 (80 mmol L^{-1}) was much more superfluous for the degradation of MB (0.2 mmol L^{-1}), so the production of •OH may be steady-state and the $[^{\bullet}OH]_{surf}$ can be regarded as a constant.

Meanwhile, as the MB concentration did not decrease quickly during the degradation (Fig. 6A), its instantaneous adsorbed amount can also be assumed as constant. Therefore, the MB degradation process can be described by the zero-order equation:

$$\frac{d[\equiv\text{M–OMB}]}{dt} = -kq[^{\bullet}\text{OH}]_{\text{surf}} \quad (5)$$

$$k_{\text{app}} = kq[^{\bullet}\text{OH}]_{\text{surf}} \quad (6)$$

$$C_0 - C_t = k_{\text{app}}t \quad (7)$$

where C_0 and C_t are the MB concentrations (mmol L^{-1}) at the initial time and reaction time t, k_{app} is zero-order apparent rate constant (mmol L^{-1} min^{-1}), q is the MB adsorbed amount on $Fe_{3-x}Cr_xO_4$ surface (mg g^{-1}), and $[^{\bullet}OH]_{surf}$ is the steady-state concentration of •OH radicals on $Fe_{3-x}Cr_xO_4$ surface (mmol g^{-1}). The k_{app} constant can be obtained directly by regressing the lines in Fig. 6A (r > 0.98, Table 3), indicating that the MB degradation was well fitted with the zero-order equation and followed the Langmuir–Hinshelwood model. The k_{app} constant increased with increase of Cr content in the catalyst (Table 3).

For AOII, as it was not adsorbed onto magnetite surface, the degradation process should not follow the Langmuir–Hinshelwood model but the Eley–Rideal mechanism (i.e. reaction of dissolved AOII molecule with •OH produced on magnetite surface, Eq. (8)) [40,41], which also can be described as a second-order reaction (Eq. (9)):

$$\text{AOII} + [^{\bullet}\text{OH}]_{\text{surf}} \rightarrow \text{product} \quad (8)$$

$$\frac{dC}{dt} = -KC[^{\bullet}\text{OH}]_{\text{surf}} \quad (9)$$

By assuming that the •OH instantaneous concentration on $Fe_{3-x}Cr_xO_4$ surface is constant, the degradation process of AOII could be described by the pseudo-first-order equation:

$$\frac{dC}{dt} = -K_{\text{app}}C \quad (10)$$

$$K_{\text{app}} = K[^{\bullet}\text{OH}]_{\text{surf}} \quad (11)$$

$$-\ln\left(\frac{C_t}{C_0}\right) = K_{\text{app}}t \quad (12)$$

where C_0 and C_t are the AOII concentrations (mmol L^{-1}) at the initial time and reaction time t, K_{app} is pseudo-first-order appear rate constant (min^{-1}), and t is degradation time (min). The K_{app} constant can be obtained from the slope of the straight lines by plotting $-\ln(C_t/C_0)$ as a function of time t, through regression. Fig. 7 shows the results of Fig. 6B plotted in the form of Eq. (12). It can be seen that the degradation process of AOII by $Fe_{2.82}Cr_{0.18}O_4$ was well fitted with the pseudo-first-order equation (r > 0.99, Table 3) rather than the zero-order equation (r < 0.97, not shown). But for $Fe_{3-x}Cr_xO_4$ with higher chromium content, their catalytic reaction processes were distinctly different and well fitted with the two-stage first-order kinetics (Fig. 7). The two-stage kinetics was composed of an initial slow degradation stage (first stage) and followed rapid degradation stage (second stage), where the K_{app} constant of the latter stage was nearly one magnitude larger than that of the former one. This two-stage kinetics has been reported

Table 3
The rate constant for the degradation of MB and acid orange II through Fenton reaction catalyzed by $Fe_{3-x}Cr_xO_4$.

Sample	MB		AOII			
	k_{app}[a]	r	K_{app}[b] (First stage)	r	K_{app}[b] (Second stage)	r
Fe_3O_4	4.15×10^{-4}	0.717	2.32×10^{-4}	0.910	2.32×10^{-4}	0.910
$Fe_{2.82}Cr_{0.18}O_4$	8.70×10^{-3}	0.981	3.20×10^{-3}	0.992	3.20×10^{-3}	0.992
$Fe_{2.67}Cr_{0.33}O_4$	1.45×10^{-2}	0.993	2.64×10^{-3}	0.990	9.59×10^{-3}	0.999
$Fe_{2.53}Cr_{0.47}O_4$	1.83×10^{-2}	0.994	2.16×10^{-3}	0.998	1.23×10^{-2}	0.998
$Fe_{2.33}Cr_{0.67}O_4$	1.92×10^{-2}	0.999	2.33×10^{-3}	0.991	1.36×10^{-2}	0.998

[a] k_{app}: zero-order constant rate for methylene blue degradation.
[b] K_{app}: pseudo-first-order rate constant for acid orange II degradation.

in detail in the previous studies [47,48]. The low K_{app} of first stage can be explained by the poor adsorption of AOII on the catalyst and the presence of high concentration of H_2O_2 in the initial stage. In this case, most produced •OH radicals could be scavenged quickly (Eq. (13)) by the surrounding H_2O_2 without reacting with the AOII molecules in the solution, resulted in a slow degradation of AOII. As the excessive H_2O_2 was partially consumed in the first stage, the produced •OH would not be rapidly scavenged and turned to attack the dye molecules, leading to the faster degradation of AOII in the second stage. The mismatching of the degradation process by $Fe_{2.82}Cr_{0.18}O_4$ with two-stage kinetics, may be related to the slow production of •OH during the whole degradation process.

$$^{\bullet}OH + H_2O_2 \rightarrow HO_2^{\bullet} + H_2O \quad (13)$$

To verify the above conclusions about two-stage kinetics, two comparison experiments were carried out by altering the initial H_2O_2 concentration or pH. Fig. 8 shows the degradation of AOII by $Fe_{2.33}Cr_{0.67}O_4$ with various initial H_2O_2 concentrations. It can be seen that with the decrease of initial H_2O_2 concentration, the K_{app} constant in the first stage gradually approached to that of the second stage and the whole degradation processes tended to be better fitted with the pseudo-first-order equation than with two-stage kinetics. This was ascribed to the decrease of initial H_2O_2 concentration and accordingly less scavenging effect of •OH radicals in the first stage. However, the decrease of initial H_2O_2 concentration inevitably slowed the AOII degradation (Fig. 8), due to the retardment of •OH production.

Fig. 9 shows the degradation of AOII by $Fe_{2.33}Cr_{0.67}O_4$ at different initial pH. The degradation processes started at pH of 9.0, 7.0 and 5.0, were well fitted with the two-stage kinetics. The degradation efficiency increased with the decrease of initial pH. When the initial pH decreased to 3.0, the degradation process changed to be well fitted with the pseudo-first-order equation (Fig. 9). Acidic pH improved the iron dissolution from magnetite surface, thus propagating the homogeneous Fenton reaction [49]. In this case, •OH was produced in the solution and it preferred to attack the dissolved AOII, rather than be scavenged by H_2O_2. Therefore, the degradation process was well fitted with the pseudo-first-order equation. These two experiments (Figs. 8 and 9) confirmed that the occur-

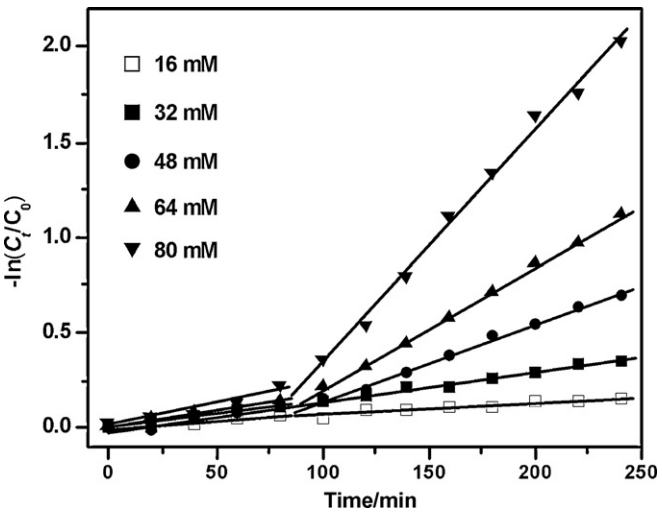

Fig. 8. Degradation of acid orange II through heterogeneous Fenton reaction by $Fe_{2.33}Cr_{0.67}O_4$ with different H_2O_2 concentrations (C_0 = 0.2 mmol L^{-1}, 1.0 g L^{-1} of $Fe_{2.33}Cr_{0.67}O_4$, 250 mL, pH 7.0, 25 °C).

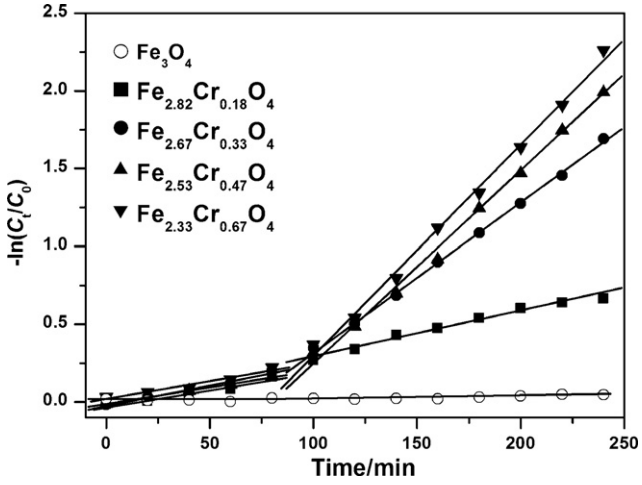

Fig. 7. Kinetics fitting of the acid orange II decolorization through heterogeneous Fenton reaction catalyzed by $Fe_{3-x}Cr_xO_4$ (C_0 = 0.2 mmol L^{-1}, 80 mmol L^{-1} of H_2O_2, 1.0 g L^{-1} of catalyst, 250 mL, pH 7.0, 25 °C).

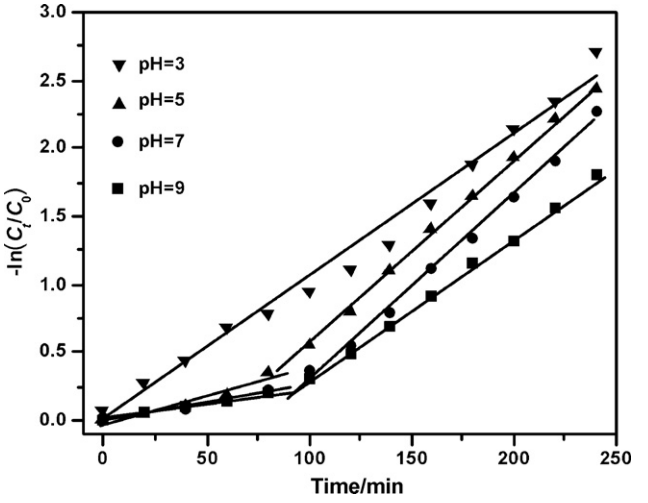

Fig. 9. Degradation of acid orange II through heterogeneous Fenton reaction by $Fe_{2.33}Cr_{0.67}O_4$ at different initial pH (C_0 = 0.2 mmol L^{-1}, 80 mmol L^{-1} of H_2O_2, 1.0 g L^{-1} of $Fe_{2.33}Cr_{0.67}O_4$, 250 mL, 25 °C).

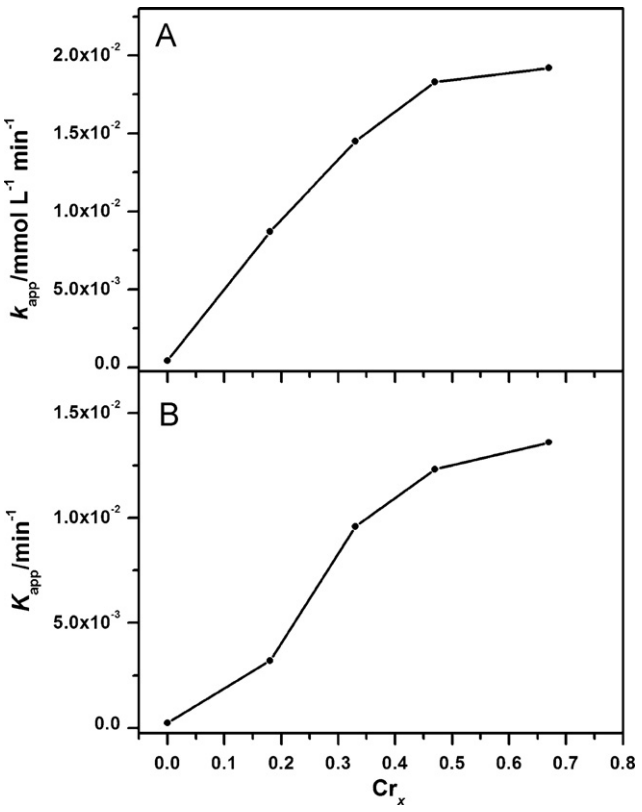

Fig. 10. Degradation rate constants for the degradation of (A) methylene blue and (B) acid orange II (second stage) with H_2O_2 in the presence of $Fe_{3-x}Cr_xO_4$.

rence of two-stage kinetics under neutral pH was related to the E–R degradation model and the high initial concentration of H_2O_2.

3.2.3. Effect of chromium substitution on catalytic activity

Table 3 shows the rate constant for the degradation of both dyes through heterogeneous Fenton reaction catalyzed by $Fe_{3-x}Cr_xO_4$ around neutral pH. Obviously, for MB and AOII (second stage), their rate constants increased with the increase of chromium content in magnetite. For MB, its decolorization relied on both the MB adsorption on catalyst surface and degradation by •OH radicals. Thus, the rate constant k_{app} was related to not only the surface •OH concentration that indicated the catalytic activity of magnetite for H_2O_2 decomposition, but also the adsorbed amount of MB that also was influenced by Cr substitution (Eq. (7)). So in MB degradation, the increase of k_{app} constant cannot exactly reflect the effect of Cr substitution on the catalytic activity of magnetite. But for AOII, because of its neglectable adsorption on magnetite surface and no obvious change of pH during the degradation, its decolorization should mainly rely on degradation. Hence, its degradation rate constant was in proportion to the •OH steady-state concentration (Eq. (11)) and therefore indicative of the catalytic activity of magnetite. Fig. 10 shows the variations of degradation rate constants with Cr substitution level in the degradation of MB and AOII (second stage). It can be seen that in AOII degradation, Cr substitution obviously increased the second-stage rate constant, indicating the enhancement of catalytic activity of magnetite. As shown by the previous research [3], the positive effect of Cr originates from the Cr^{3+} on octahedral site that can decompose H_2O_2 to create •OH and improve the electron transfer to produce Fe^{2+} during the reaction. Moreover, the increase of surface hydroxyl provides more active sites for H_2O_2 decomposition to produce •OH [45]. In Fig. 10B, for x in range of 0–0.3, chromium substitution greatly improved the catalytic activity while for x above 0.3, the improvement of catalytic activity looked less remarkable. This phenomenon may be related to the variation of cation distribution with different substitution extent. As Cr^{3+} replaces Fe^{3+} at the octahedral sites of magnetite, which was indicated by the XANES characterization, no Fe^{2+} are displaced from octahedral sites to tetrahedral sites up to $x = 0.3$ [50,51]. But for $x > 0.3$, Fe^{2+} in octahedral sites starts to move to tetrahedral sites and the moving number increases with the increase of substitution level [50,51]. Based on the fact that Fe^{2+} is the active species for the Fenton reaction and the catalytic activity relies on the octahedral cations rather than the tetrahedral ones, the transfer of Fe^{2+} from octahedral sites to tetrahedral sites can explain less increase of catalytic activity when x is above 0.3. For MB, the increasing trend of rate constant in low substitution level ($x < 0.3$) was a bit different from that in AOII degradation, which was possibly ascribed to different adsorption behaviors between MB and AOII.

4. Conclusions

The present study has investigated the catalytic activity of chromium substituted magnetite in the heterogeneous Fenton degradation of different types of dyes, MB (cationic dye) and AOII (anionic dye). Cr cations in valency of +3 occupy the octahedral sites of magnetite, increasing the BET surface area and superficial hydroxyl amount. MB adsorption on magnetite is enhanced by chromium substitution, while AOII cannot be adsorbed onto $Fe_{3-x}Cr_xO_4$. Cr substitution greatly increases the catalytic activity of magnetite in the heterogeneous Fenton reaction, but its enhancement extent depends on the chromium substitution level. The degradation of these two dyes follows different mechanisms and kinetics. The obtained novel insights are of high importance for the utilization of substituted magnetite in the field of wastewater treatment.

Acknowledgments

This is contribution No. IS-1459 from GIG CAS. We would like to thank Shanghai Synchrotron Radiation Facility (SSRF) for providing us the beam time for the XANES measurement. This work is financially supported by National Natural Science Foundation of China (grant nos. 40773060 and 41172045).

Appendix A. Supplementary data

Supplementary data associated with this article can be found, in the online version, at doi:10.1016/j.cej.2012.03.001.

References

[1] R.C.C. Costa, M.F.F. Lelis, L.C.A. Oliveira, J.D. Fabris, J.D. Ardisson, R.R.V.A. Rios, C.N. Silva, R.M. Lago, Novel active heterogeneous Fenton system based on $Fe_{3-x}M_xO_4$ (Fe, Co, Mn, Ni): the role of M^{2+} species on the reactivity towards H_2O_2 reactions, J. Hazard. Mater. 129 (2006) 171–178.
[2] J.H. Deng, J.Y. Jiang, Y.Y. Zhang, X.P. Lin, C.M. Du, Y. Xiong, $FeVO_4$ as a highly active heterogeneous Fenton-like catalyst towards the degradation of orange II, Appl. Catal. B: Environ. 84 (2008) 468–473.
[3] F. Magalhaes, M.C. Pereira, S.E.C. Botrel, J.D. Fabris, W.A. Macedo, R. Mendonca, R.M. Lago, L.C.A. Oliveira, Cr-containing magnetites $Fe_{3-x}Cr_xO_4$: the role of Cr^{3+} and Fe^{2+} on the stability and reactivity towards H_2O_2 reactions, Appl. Catal. A: Gen. 332 (2007) 115–123.
[4] R.C.C. Costa, M. de Fatima, F. Lelis, L.C.A. Oliveira, J.D. Fabris, J.D. Ardisson, R.R.V.A. Rios, C.N. Silva, R.M. Lago, Remarkable effect of Co and Mn on the activity of $Fe_{3-x}M_xO_4$ promoted oxidation of organic contaminants in aqueous medium with H_2O_2, Catal. Commun. 4 (2003) 525–529.
[5] E.G. Garrido-Ramirez, B.K.G. Theng, M.L. Mora, Clays and oxide minerals as catalysts and nanocatalysts in Fenton-like reactions–a review, Appl. Clay Sci. 47 (2010) 182–192.
[6] T.L. Jentzsch, C.L. Chun, R.S. Gabor, R.L. Penn, Influence of aluminum substitution on the reactivity of magnetite nanoparticles, J. Phys. Chem. C 111 (2007) 10247–10253.
[7] S.J. Yang, H.P. He, D.Q. Wu, D. Chen, X.L. Liang, Z.H. Qin, M.D. Fan, J.X. Zhu, P. Yuan, Decolorization of methylene blue by heterogeneous Fenton reaction

using $Fe_{3-x}Ti_xO_4$ ($0 \le x \le 0.78$) at neutral pH values, Appl. Catal. B: Environ. 89 (2009) 527–535.
[8] X.L. Liang, S.Y. Zhu, Y.H. Zhong, J.X. Zhu, P. Yuan, H.P. He, J. Zhang, The remarkable effect of vanadium doping on the adsorption and catalytic activity of magnetite in the decolorization of methylene blue, Appl. Catal. B: Environ. 97 (2010) 151–159.
[9] C.G. Ramankutty, S. Sugunan, Surface properties and catalytic activity of ferrospinels of nickel, cobalt and copper, prepared by soft chemical methods, Appl. Catal. A: Gen. 218 (2001) 39–51.
[10] M. Sorescu, A. Grabias, D. Tarabasanu-Mihaila, L. Diamandescu, Influence of cobalt and nickel substitutions on populations, hyperfine fields, and hysteresis phenomenon in magnetite, J. Appl. Phys. 9 (1) (2002) 8135–8137.
[11] L.C.A. Oliveira, J.D. Fabris, R.R.V.A. Rios, W.N. Mussel, R.M. Lago, $Fe_{3-x}Mn_xO_4$ catalysts: phase transformations and carbon monoxide oxidation, Appl. Catal. A: Gen. 259 (2004) 253–259.
[12] C.G. Ramankutty, S. Sugunan, B. Thomas, Study of cyclohexanol decomposition reaction over the ferrospinels $A_{(1-x)}Cu_{(x)}Fe_{(2)}O_{(4)}$ (A = Ni or Co and $x = 0$, 0.3, 0.5, 0.7 and 1), prepared by "soft" chemical methods, J. Mol. Catal. A: Chem. 187 (2002) 105–117.
[13] R.C. Wu, J.H. Qu, Removal of azo dye from water by magnetite adsorption-Fenton oxidation, Water Environ. Res. 76 (2004) 2637–2642.
[14] M.A. Al-Ghouti, M.A.M. Khraisheh, M.N.M. Ahmad, S. Allen, Adsorption behaviour of methylene blue onto Jordanian diatomite: a kinetic study, J. Hazard. Mater. 165 (2009) 589–598.
[15] Q. Wang, C.C. Chen, D. Zhao, W.H. Ma, J.C. Zhao, Change of adsorption modes of dyes on fluorinated $TiO_{(2)}$ and its effect on photocatalytic degradation of dyes under visible irradiation, Langmuir 24 (2008) 7338–7345.
[16] K. Chhor, J.F. Bocquet, C. Colbeau-Justin, Comparative studies of phenol and salicylic acid photocatalytic degradation: influence of adsorbed oxygen, Mater. Chem. Phys. 86 (2004) 123–131.
[17] M.K. Azer, R.J. Stern, Neoproterozoic (835–720 Ma) serpentinites in the Eastern Desert, Egypt: fragments of forearc mantle, J. Geol. 115 (2007) 457–472.
[18] R.B. Garcia-Reyes, J.R. Rangel-Mendez, Adsorption kinetics of chromium(III) ions on agro-waste materials, Bioresour. Technol. 101 (2010) 8099–8108.
[19] C.A.P. Almeida, C. Machado, N.A. Debacher, Adsorption of methylene blue as a model for the use of Barro Branco as an alternative adsorbent for color removal, Surf. Colloid Sci. 128 (2004) 278–282.
[20] S.H. Tian, Y.T. Tu, D.S. Chen, X. Chen, Y. Xiong, Degradation of acid orange II at neutral pH using $Fe_2(MoO_4)_3$ as a heterogeneous Fenton-like catalyst, Chem. Eng. J. 169 (2011) 31–37.
[21] J.X. Chen, L.Z. Zhu, Oxalate enhanced mechanism of hydroxyl-Fe-pillared bentonite during the degradation of orange II by UV-Fenton process, J. Hazard. Mater. 185 (2011) 1477–1481.
[22] B.H. Moon, Y.B. Park, K.H. Park, Fenton oxidation of orange II by pre-reduction using nanoscale zero-valent iron, Desalination 268 (2011) 249–252.
[23] W. Yu, T.L. Zhang, H. Zhang, X.J. Qiao, L. Yang, Y.H. Liu, The synthesis of octahedral nanoparticles of magnetite, Mater. Lett. 60 (2006) 2998–3001.
[24] W.G. Hu, Y.L. Su, D.J. Sun, C.G. Zhang, Studies on zero point of charge and permanent charge density of Mg–Fe hydrotalcite-like compounds, Langmuir 17 (2001) 1885–1888.
[25] J.X. Chen, L.Z. Zhu, UV-Fenton discolouration and mineralization of orange II over hydroxyl-Fe-pillared bentonite, J. Photochem. Photobiol. A 188 (2007) 56–64.
[26] J.Y. Feng, X.J. Hu, P.L. Yue, Discoloration and mineralization of orange II using different heterogeneous catalysts containing Fe: a comparative study, Environ. Sci. Technol. 38 (2004) 5773–5778.
[27] J.Y. Park, J.H. Lee, K.J. Kim, Ionic distribution and related electronic properties in $V_xFe_{3-x}O_4$ thin films studied by using Mossbauer and X-ray photoelectron spectroscopy, J. Korean Phys. Soc. 53 (2008) 695–699.
[28] A. Pradeep, G. Chandrasekaran, FTIR study of Ni, Cu and Zn substituted nanoparticles of $MgFe_2O_4$, Mater. Lett. 60 (2006) 371–374.
[29] H.M. Wang, G.S. Henderson, Investigation of coordination number in silicate and germanate glasses using O K-edge X-ray absorption spectroscopy, Chem. Geol. 213 (2004) 17–30.
[30] M. Wilke, F. Farges, P.E. Petit, G.E. Brown, F. Martin, Oxidation state and coordination of Fe in minerals: an FeK-XANES spectroscopic study, Am. Mineral. 86 (2001) 714–730.
[31] A. Pantelouris, H. Modrow, M. Pantelouris, J. Hormes, D. Reinen, The influence of coordination geometry and valency on the K-edge absorption near edge spectra of selected chromium compounds, Chem. Phys. 300 (2004) 13–22.
[32] D. Lenaz, H. Skogby, F. Princivalle, U. Halenius, Structural changes and valence states in the $MgCr_2O_4$–$FeCr_2O_4$ solid solution series, Phys. Chem. Miner. 31 (2004) 633–642.
[33] D. Thickett, M. Odlyha, Application of thermomagnetometry to corrosion studies of archaeological iron, J. Therm. Anal. Calorim. 80 (2005) 565–571.
[34] Y. Zhang, M. Yang, X.M. Dou, H. He, D.S. Wang, Arsenate adsorption on an Fe–Ce bimetal oxide adsorbent: role of surface properties, Environ. Sci. Technol. 39 (2005) 7246–7253.
[35] K. Nagaveni, G. Sivalingam, M.S. Hedge, G. Madras, Solar photocatalytic degradation of dyes: high activity of combustion synthesized nano TiO_2, Appl. Catal. B: Environ. 48 (2004) 83–93.
[36] Y.H. Zhang, G.X. Xiong, N. Yao, W.S. Yang, X.Z. Fu, Preparation of titania-based catalysts for formaldehyde photocatalytic oxidation from $TiCl_4$ by the sol–gel method, Catal. Today 68 (2001) 89–95.
[37] R.M. Cornell, U. Schwertmann, The Iron Oxides: Structure, Properties, Reactions, Occurrences and Uses, Wiley-VCH Verlag GmbH, D-69469 Weinheim (Federal Republic of Germany), 2003.
[38] U. Schwertmann, E. Wolska, The influence of aluminum on iron-oxides.15. Al-for-Fe substitution in synthetic lepidocrocite, Clays Clay Miner. 38 (1990) 209–212.
[39] R.G. Harris, J.D. Wells, B.B. Johnson, Selective adsorption of dyes and other organic molecules to kaolinite and oxide surfaces, Colloid Surf. A 180 (2001) 131–140.
[40] C.A.P. Almeida, N.A. Debacher, A.J. Downs, L. Cottet, C.A.D. Mello, Removal of methylene blue from colored effluents by adsorption on montmorillonite clay, J. Colloid Interface Sci. 332 (2009) 46–53.
[41] S.S. Chou, C.P. Huang, Decomposition of hydrogen peroxide in a catalytic fluidized-bed reactor, Appl. Catal. A: Gen. 185 (1999) 237–245.
[42] Y.P. Zhao, H.Y. Hu, Photo-Fenton degradation of 17 beta-estradiol in presence of alpha-FeOOHR and H_2O_2, Appl. Catal. B: Environ. 78 (2008) 250–258.
[43] T. Maezono, M. Tokumura, M. Sekine, Y. Kawase, Hydroxyl radical concentration profile in photo-Fenton oxidation process: generation and consumption of hydroxyl radicals during the discoloration of azo-dye orange II, Chemosphere 82 (2011) 1422–1430.
[44] H. Zhang, H. Fu, D.B. Zhang, Degradation of CI acid orange 7 by ultrasound enhanced heterogeneous Fenton-like process, J. Hazard. Mater. 172 (2009) 654–660.
[45] S.S. Lin, M.D. Gurol, Catalytic decomposition of hydrogen peroxide on iron oxide: kinetics, mechanism, and implications, Environ. Sci. Technol. 32 (1998) 1417–1423.
[46] H.S. Son, J.K. Im, K.D. Zoh, A Fenton-like degradation mechanism for 1,4-dioxane using zero-valent iron ($Fe^{(0)}$) and UV light, Water Res. 43 (2009) 1457–1463.
[47] T. Zhou, Y.Z. Li, J. Ji, F.S. Wong, X.H. Lu, Oxidation of 4-chlorophenol in a heterogeneous zero valent iron/H_2O_2 Fenton-like system: kinetic, pathway and effect factors, Sep. Purif. Technol. 62 (2008) 551–558.
[48] L.J. Xu, J.L. Wang, A heterogeneous Fenton-like system with nanoparticulate zero-valent iron for removal of 4-chloro-3-methyl phenol, J. Hazard. Mater. 186 (2011) 256–264.
[49] X. Zeng, K. Hanna, A.T. Lemley, Cathodic Fenton degradation of 4,6-dinitro-o-cresol with nano-magnetite, J. Mol. Catal. A: Chem. 339 (2011) 1–7.
[50] M. Robbins, G.K. Wertheim, R.C. Sherwood, D.N. Buchanan, Magnetic properties and site distributions in system $FeCr_2O_4$–Fe_3O_4($Fe^{2+}Cr_{2-x}Fe_x{}^{3+}O_4$), J. Phys. Chem. Solids 32 (1971) 717–729.
[51] H.N. Ok, L.S. Pan, B.J. Evans, Fe-57 Mossbauer study of chromium-doped magnetite, $Fe_{3-x}Cr_xO_4$ ($0 \le x \le 0.5$) above Verwey transition, Phys. Rev. B 17 (1978) 85–90.